Available online at www.sciencedirect.com
SCIENCE DIRECT
Polymer 46 (2005) 10960–10969
polymer
www.elsevier.com/locate/polymer

Effects of sodium benzoate on distributions of lamellar structures of sheared isotactic polypropylene: A study using small angle synchrotron X-ray scattering

Peng-wei Zhu*, Jason Tung, Graham Edward

Department of Materials Engineering, CRC for Polymers, Monash University, Room 102, Building 36, Clayton, Vic. 3800, Australia

Received 15 February 2005; received in revised form 1 September 2005; accepted 7 September 2005
Available online 23 September 2005

Abstract

Small-angle X-ray scattering (SAXS) studies were carried out to investigate effects of sodium benzoate (SB) on the shear-induced distributions of lamellar structures through the depth direction of injection-moulded isotactic polypropylene (iPP) plates, using the micro beam available from a synchrotron to gain good spatial resolution. It was found that in the presence of SB, the shish–kebab structure emerges over a broader range to include regions in which a random arrangement of crystalline lamellae is found without SB. The oriented crystalline lamellae are even found in positions that are very close to the core center. The SB-induced shish–kebab structure under low levels of shear flow is attributed to lower free energy barriers for the coil-to-stretch transition and shorter times to start the crystallization. The effect of SB on the lamellar dimensions is significant only in the core region, and only when the concentration of SB is sufficiently high. A down-U distribution of the long spacing is found, which is mainly ascribed to the variation of thickness of crystalline lamellae with the depth. The results show that a higher level of lamellar orientation is not necessarily accompanied by a higher degree of linear crystallinity.

Keywords: Lamellar distribution; Nucleating agent; Shear flow

1. Introduction

Flow fields, including shear, elongation, and mixed, can effectively introduce different levels of molecular and lamellar anisotropy to semicrystalline polymer melts at different stages of processing [1,2]. As a result, the processing history of flow on a semicrystalline polymer melt can affect the morphology, morphological distribution, and product properties as well. In most polymer processing operations, both the morphology and its distribution through the resultant polymer products are strongly influenced by the orientation induced by the flow in the molten state. In particular, the flow-induced crystallization of polymer melts can result in the formation of a so-called shish–kebab structure in semicrystalline polymers under appropriate conditions [3–6]. This special kind of chain crystalline assembly consists of folded-chain lamellae or kebabs periodically held together by fibrillar crystals or shishes [3–13]. The formation of such a structure is considered to be a direct consequence of a coil-to-stretch transition of polymer chains in the melt crystallization when the shear rate exceeds a critical value [3,7]. It has been predicted and observed that longer coiled-chains (longer than a critical length) of a polydisperse polymer melt can stretch to the shishes while at the same flow rate shorter coiled-chains epitaxially grow into the kebabs [5–7]. It has been found that the flow fields are always essential for the formation of the shish, whereas the kebabs can grow on the shish in the absence of any flow [7,10,11].

Injection-moulded isotactic polypropylene (iPP) articles have a multiple layer or skin-core structure [1,2,14–19]. The very thin skin region is essentially characterized to be an amorphous phase. The broad core region contains spherulites because the lower cooling rate and lower shear-strain history in the region allow a complete relaxation of chain molecules. The shish–kebab structure has been frequently detected in the surface region of sheared iPP [1,20,21]. A similar structure, 'parent–daughter' model, is also proposed. [22–25].

This paper is to explore the effects of sodium benzoate (SB), a nucleating agent, on the lamellar structures of injection-moulded iPP plates using micro beam of synchrotron small-angle X-ray scattering (SAXS) and to establish the corresponding distributions of the lamellar structures

* Corresponding author. Tel.: +61 3 990 59981.
E-mail address: peng.zhu@spme.monash.edu.au (P.- Zhu).

0032-3861/$ - see front matter © 2005 Elsevier Ltd. All rights reserved.
doi:10.1016/j.polymer.2005.09.023

along the shear flow field through the thickness of the plate. A recent study has shown that the shish–kebab structure of the sheared iPP can be distributed over a much broader range of the flow field in the presence of SB [26]. For iPP/SB films that were prepared from dilute solutions in the absence of flow field, methyl side chains in (010) and (110) crystal planes of iPP are found to be spatially organized as linear gratings with different periodicities [27]. Heteroepitaxial crystallization occurs when foreign substrates specifically match these distances. For the melt crystallization of sheared iPP in the presence of SB, however, the lamellar structures of iPP and corresponding distributions have not been reported.

2. Experimental

A commercial iPP (M_w=260,000, M_n=41,200) and SB were kindly provided by Basell. SB was mixed in a small single screw extruder with iPP at a SB concentration of 4.0 wt% to produce a masterbatch. The masterbatch extrudate was pelletised and further extruded to improve the dispersion and distribution of the SB. This was then mixed with further iPP in the extruder to produce different concentrations of SB before injection moulding. Rectangular plates of iPP were injection moulded with conditions as follows: melt temperature 220 °C, mold temperature 60 °C, holding pressure 250 bar, holding time 3.8 s, cooling time 40 s and flow front velocity 2 cm/s through the cavity. The injection moulded iPP specimens were cut at a central position away from the gate, as shown in Fig. 1. These specimens were named iPP-0.0, iPP-0.1, iPP-0.4, and iPP-1.2, corresponding to the SB concentrations of none, 0.1, 0.4, and 1.2 wt%, respectively.

The X-ray scattering experiments were performed at room temperature at the Australian national beamline facility (ANBF), a synchrotron beam-line at the Photon Factory in Tsukuba, Japan. The ANBF is installed on a bending magnet port, and delivers monochromatic synchrotron X-rays in the energy range 4.5–20 keV to the experimental station in a hutch. The instrument has a multi-configuration vacuum diffractometer that uses image plates as its detector system. The square-shaped micro-beam had a dimension of 200×200 μm^2. A wavelength of 2.0 Å was employed to record 2D SAXS image patterns.

Measurements were performed with the primary beam being perpendicular to the flow direction and the scattering being measured along a direction normal to the layered planes in the moulding. The beam passed through the specimen and the illuminated zone was changed with a vertical shift of the sample holder along the direction of plate thickness. Only one half width of each specimen was illuminated on the assumption that the morphology at the same distance from the surfaces of the plate is the same. For all specimens, the first measurement was always taken with the beam centre 100 μm from the surface. The intensity at 100 μm is, therefore, low simply because the illuminated area is small. This step should not be taken as a measurement of the skin as the X-ray beam cannot access the specimen skin in the present experiments. The scattered intensity was then presented as a function of scattering vector q where $q=4\pi \sin(\theta)/\lambda$. Scattering without the specimen was recorded as a background scattering I_b, to enable correction of measured SAXS patterns.

3. Results and discussion

Fig. 2 shows the 2D SAXS image patterns through the depth of iPP-0.0 and iPP-0.1. These images represent the raw patterns without background correction. As the distance from

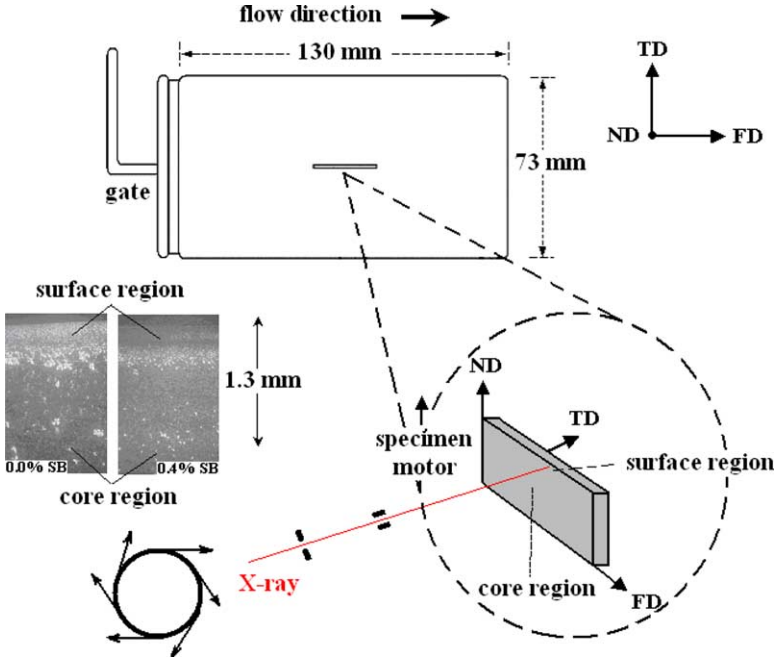

Fig. 1. A schematic diagram of an injection-moulded plate and the injection moulded iPP specimen cut at a central position away from the gate. The plane of the specimens is parallel to the flow direction and the X-ray beam is then normal to the flow direction.

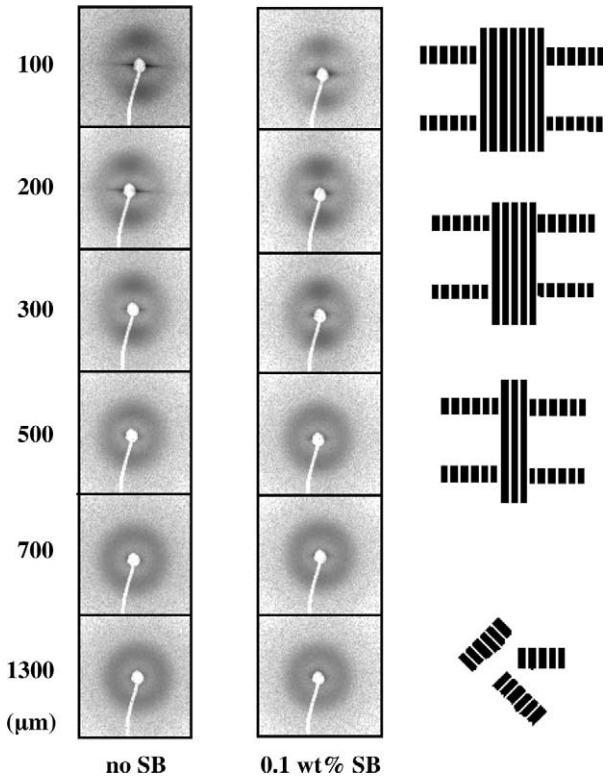

Fig. 2. 2D SAXS image patterns at different distances from the surface of plates for iPP-0.0 and iPP-0.1. The flow direction is vertical. The schematic drawing illustrates the type of morphology that could lead to the patterns, with a central shish and lateral lamellar kebabs giving way to an isotropic lamellar arrangement further away from the surface.

the surface increased from 100 to 300 μm, two scattering maxima along and normal to the flow direction are observed, which indicates a morphological orientation. However, the equatorial maximum at 300 μm decreases significantly whereas the meridional maximum shows, qualitatively, not much change. The equatorial and meridional maxima of iPP-0.0 and iPP-0.1 are weak at 500 μm. The effect of SB on the 2D SAXS pattern becomes visibly differential when the distance from the surface is increased to 700 μm. It can be seen that the image pattern of iPP-0.0 at 700 μm shows almost isotropic features. At the same position, however, the equatorial scattering is detectable from iPP-0.1. Not that the meridional maximum of iPP-0.0 at 700 μm remains, at least visibly, the same. The image pattern of iPP-0.1 shows isotropic feature when the distance is increased to 1300 μm, the center of plate thickness.

The equatorial maximum is attributed to a bundle of the shishes parallel to the flow direction whereas the meridional maximum is attributed to the fold chain kebabs perpendicular to the flow direction [28]. The SAXS image patterns presented here reveal the development of the shish–kebab structure through the depth of the injection-moulded iPP plate. The number and size of the shish could change as the level of effective level of shear flow imposed on the iPP melt rapidly attenuates with increasing thickness of the plate toward the core center. It is particularly noted that in the presence of small amount of SB the shish–kebab structure emerges at 700 μm at which the unoriented structure is feature in the absence of SB.

The effects of SB on the distribution of the shish–kebab structures along the shear flow field become significant as the concentration of SB is further increased. Fig. 3 shows the 2D SAXS image patterns through the plate thickness of iPP-0.4 and iPP-1.2. As can be seen, the magnitude of the scattering maxima is strongly dependent on the concentration of SB. The oriented crystallization is remarkably enhanced at these concentrations of SB, although all samples were injection-moulded under the same conditions. Compared with the image patterns of iPP-0.1 at 500 and 700 μm, the equatorial and meridional maxima can be more easily observed from iPP-0.4 and become much more distinct in iPP-1.2. Furthermore, both the equatorial and the meridional maxima of iPP-1.2 can be seen even at 900 μm from the surface. It is worth pointing out that for these 2600 μm thick samples, 900 μm from the surface is well within what is generally regarded as the isotropic core region, although this is clearly not entirely the case for iPP-1.2. Like iPP-0.0, isotropic image patterns are found for iPP-0.4 and iPP-1.2 at 1300 μm. The SAXS image patterns indicate a random arrangement of lamellar stacks at 1300 μm, where the shear flow is generally considered to be insignificant.

In order to describe quantitatively the effect of SB on the distribution of lamellar dimensions through the thickness of plates, the 2D SAXS image patterns are sectioned into two parts, as illustrated in Fig. 4, for the calculation of oriented intensities, namely meridional scattering I_m and equatorial scattering I_e. The background scattering was subtracted from the image patterns of the samples. The 'box size' or integration area of PPDA software was set to be the same for all

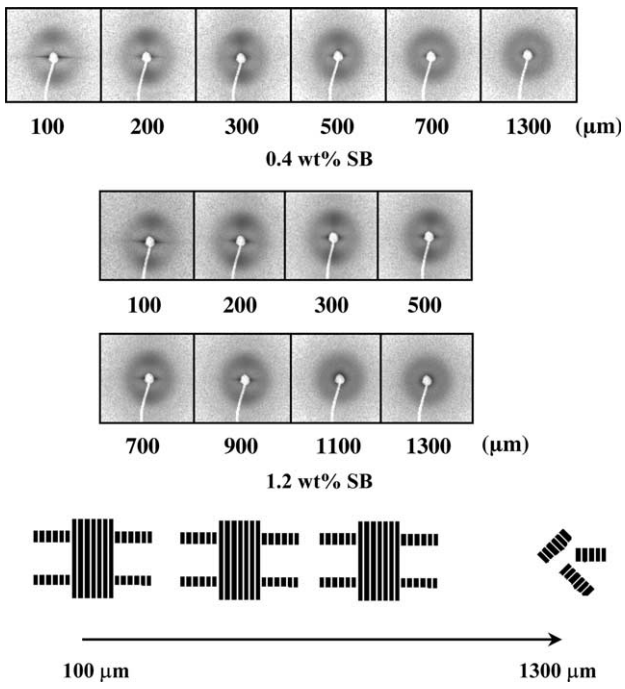

Fig. 3. 2D SAXS image patterns at different distances from the surface of plates for iPP-0.4 and iPP-1.2. The flow direction is vertical. The schematic drawing illustrates the type of morphology that could lead to the patterns.

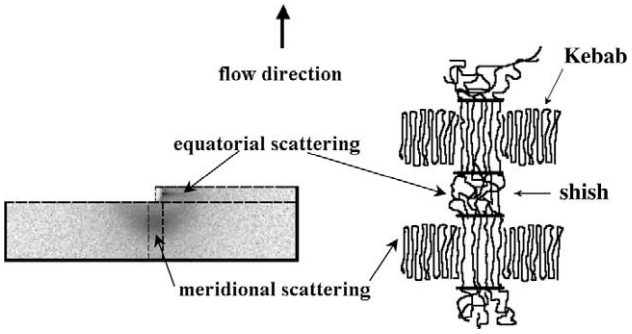

Fig. 4. Sections of 2D SAXS image patterns showing the calculation of box-integrated SAXS intensities along the equatorial and meridional directions. The flow direction is vertical. The schematic drawing shows the type of morphology that could lead to the patterns.

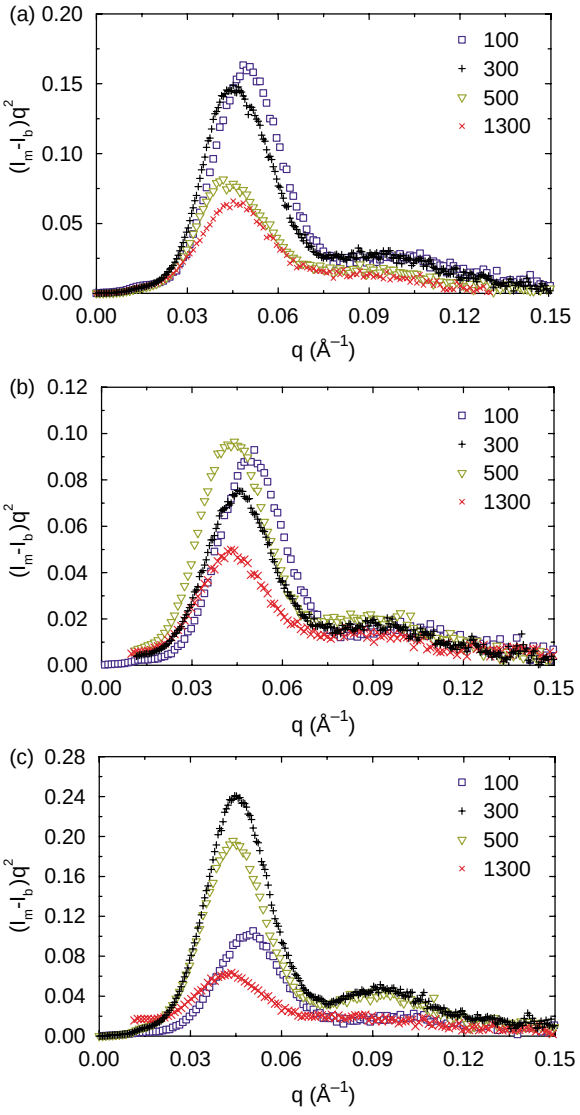

Fig. 5. Lorentz-corrected SAXS intensity profiles along the meridional direction at selected depths of injection-moulded iPP plates: (a) iPP-0.0, (b) iPP-0.4, and (c) iPP-1.2.

the positions of each sample to enable quantitative comparison. The broad I_m is typically what is attributed as being due to the lamellar morphology in a partially oriented polymer system. Fig. 5 presents Lorentz-corrected I_m profiles at the selected distances from the surface of the plate. It should be pointed out that the growth rate of polymer crystallization is independent of the type of nucleation, and folded chains can grow from points, surfaces, or be row nucleated [29]. Both oriented crystalline lamellae and randomly distributed crystalline lamellae could coexist in the positions at which the shish–kebab structure is revealed.

The distributions of the areas under I_m and I_e patterns, $\langle I_m \rangle$ and $\langle I_e \rangle$, are shown in Fig. 6. The areas at 100 μm of all samples were not included because only part of the position was radiated and the integrated intensity obtained cannot be compared quantitatively. As can be seen from Fig. 6, the magnitude of $\langle I_e \rangle$ does not vary greatly with depth through the plate (except for one position of iPP-0.0, which may be associated with the position sensitivity and chance experimental variation). In general, the distribution of $\langle I_e \rangle$ shows a somewhat down-U curvature for all the samples, i.e., $\langle I_e \rangle$ slightly increases from

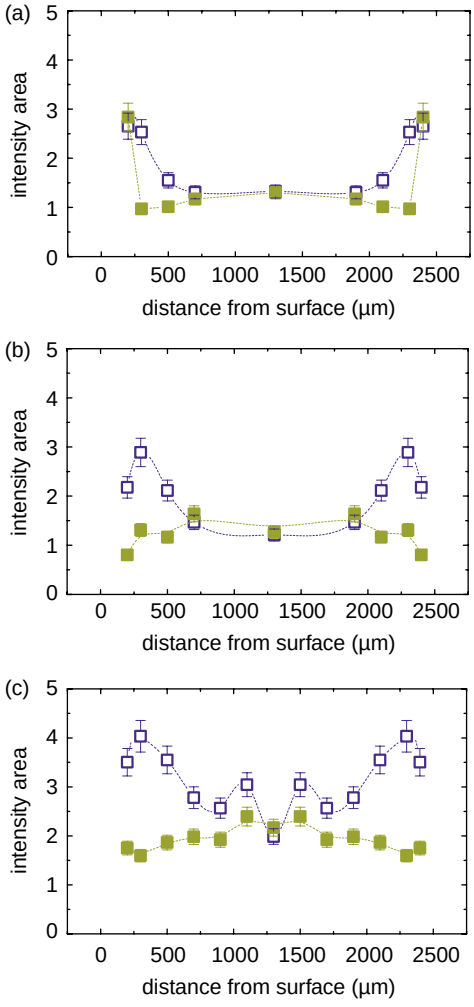

Fig. 6. Distributions of intensity areas of equatorial (filled symbols) and meridional (open symbols) scattering through the depth direction of injection-moulded iPP plates: (a) iPP-0.0, (b) iPP-0.4, and (c) iPP-1.2.

the surface region to the core centre. This trend is particularly noticeable for iPP-1.2. In the overall range, the values of $\langle I_e \rangle$ of iPP-1.2 are greater than those of iPP-0.0. In particular, the value of $\langle I_e \rangle$ obtained from the core center of iPP-1.2 is ≈ 2.2, greater than ≈ 1.3 from the core of iPP-0.0. Since, there is no shear flow at the core center, the increase in $\langle I_e \rangle$ of iPP-1.2 should not be attributed to the formation of any fibrillar structure. It is suggested that the formation of SB aggregates and/or SB modified iPP lamellae should be taken into account. The distribution of $\langle I_m \rangle$ reveals the influence of shear flow on the development of lamellar morphology. The higher value of $\langle I_m \rangle$ is ascribed to a number of changes in lamellar structures due to the addition of SB. They include the higher density, the higher level of partial orientation, and the larger number. Particularly, the decline of $\langle I_m \rangle$ with the depth becomes slower with increasing concentration of SB, indicating that the portion of oriented crystalline lamellae distributes over a broader range of the depth. Note that at the core center, $\langle I_m \rangle$ and $\langle I_e \rangle$ have almost the same values within experimental error.

The fraction of orientated crystalline lamellae can be broadly defined as follows:

$$X_{or} = \frac{\text{oriented scattering intensity}}{\text{total scattering intensity}} \tag{1}$$

The total scattering contains two contributions. The first comes from the amorphous regions and the second from the crystalline lamellae. The scattering of the crystalline phase of iPP formed under the influence of shear flow is contributed from the oriented and unoriented crystalline lamellae. In the present work, the total scattering obtained from the core center (1300 μm) contains contributions from the amorphous chains and unoriented crystalline lamellae only, and can thus be taken as representative of the total scattering. Accordingly, the fraction of orientated crystalline lamellae can be written as follows:

$$X_{or} = \frac{\langle I_m \rangle - \langle I_m(c) \rangle}{\langle I_m \rangle} \tag{2}$$

where $\langle I_m(c) \rangle$ is the area at the core center. Physically, X_{or} gives a measure of the relative level of orientation of crystalline lamellae.

Fig. 7 shows the distribution of X_{or} through the depth of the plate. In the shear zone, the maximum fraction of oriented crystalline lamellae increases from 55% for iPP-0.0 to 65% for iPP-1.2. As the concentration of SB increases, higher fractions of oriented crystalline lamellae are found over a broader range. If $X_{or} = 30\%$ is chosen as a criterion, the upper limits over which the fraction of oriented crystalline lamellae is smaller than 30% are 300, 700, and 1100 μm, corresponding to iPP-0.0, iPP-0.4, and iPP-1.2, respectively.

The structural parameters of lamellae were calculated using a one-dimensional correlation function [30]. The lamellar stacks are assumed to be oriented perfectly within an infinite stack. The scattering from such an ideal stack should be a pair of discrete peaks along the stacking direction. Since, the lamellar stacks in a real system cannot be perfectly parallel

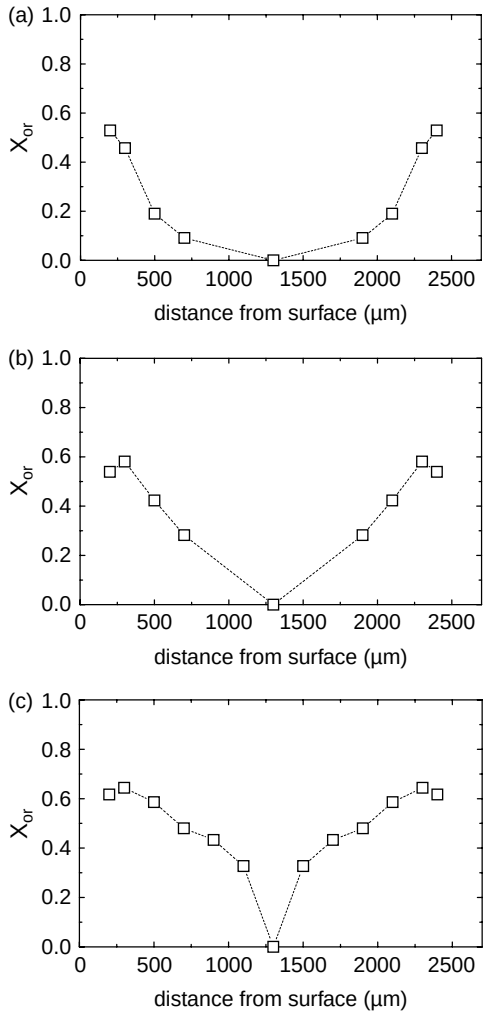

Fig. 7. Distributions of fraction of oriented crystalline lamellae along the flow direction through the depth direction of injection-moulded iPP plates: (a) iPP-0.0, (b) iPP-0.4, and (c) iPP-1.2.

to each other, nor infinite, the scattering in a reciprocal space is actually spread over an area of the reflecting sphere, this area being proportional to q^2. The Lorentz correction is used to correct a system so as to be a perfect orientation in the analysis [29]. The correlation function can be applied for the meridional intensity distribution of any partially oriented system in the same way as for an isotropic system, except for a completely orientated case like fibers [31].

The normalized one-dimensional correlation function is defined as [30,32]

$$\gamma(z) = \frac{\int_0^\infty [I_m(q) - I_t - I_b(q)] q^2 \cos(qz) dq}{Q_I} \tag{3}$$

where $Q_I = \gamma(0)$ is a scattering invariant and I_t is the background intensity arising from thermal density fluctuations. For a two-phase system with a sharp boundary, Q_I is given by

$$Q_I = \int_0^\infty [I_m(q) - I_t(q) - I_b(q)] q^2 dq = A\phi(1-\phi)\Delta\eta^2 \tag{4}$$

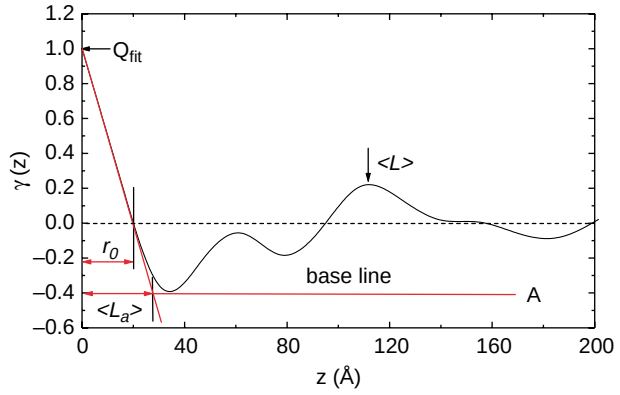

Fig. 8. A typical one-dimensional correlation function along the meridional direction at 100 μm from the surface of an injection-moulded iPP-0.4 plate.

where A is a constant related to experimental conditions. The subtraction of I_t from the measured intensity $I_m(q)$ is essential for the application of the one-dimensional correlation function. The magnitude of I_t can be estimated for the present work by the application of the pinhole-smeared form of modified Porod's law [33,34]. The q range used to evaluate the thermal density fluctuation is 0.1–0.12 $Å^{-1}$. In the present work, the scattered intensity arising from thermal density fluctuations is very small.

Fig. 8 shows a typical plot of the correlation function and related parameters from the meridional scattering. Since, the lamellar dimensions are not a constant throughout the whole sample but have distributions [35], the values obtained are average ones. The average value of the long spacing, $\langle L\rangle = \langle L_c\rangle + \langle L_a\rangle$, can be obtained from the first maximum of $\gamma(z)$. $\langle L_c\rangle$ and $\langle L_a\rangle$ are the average thicknesses of the crystalline and amorphous lamellae, respectively. For $x_l \geq 0.5$, the intersection of the linear fit with $\gamma(z)=0$ is

$$r_0 = \langle L_c\rangle(1-x_l) = \langle L_a\rangle x_l \tag{5}$$

and the magnitude of the 'baseline' is defined as

$$A = \frac{Q_{fit}(1-x_l)}{x_l} \tag{6}$$

In Fig. 8, the degree of linear crystallinity x_l is assumed to be larger than 0.5. For $x_l < 0.5$, x_l in the above equations is replaced by $(1-x_l)$. The degree of linear crystallinity, which represents the fraction of crystalline lamellae in individual stacks, is calculated accordingly by

$$x_l = \frac{\langle L_c\rangle}{\langle L_c\rangle + \langle L_a\rangle} = \frac{\langle L_c\rangle}{\langle L\rangle} \tag{7}$$

Fig. 9 shows the distribution of long spacing through the depth. The long spacing is calculated by application of Bragg's law, $\langle L_{Bragg}\rangle$, and by the correlation function, $\langle L_{CF}\rangle$. In general, the distribution of $\langle L\rangle$ tends to be a weak down U-shape. A significant increase in $\langle L\rangle$ is only observed when the concentration of SB is increased to 1.2 wt%. Note that $\langle L_{Bragg}\rangle$ is always greater than $\langle L_{CF}\rangle$. This inequality is caused by the distribution of long spacing in the material and thus the morphology deviates from the ideal two-phase model [35].

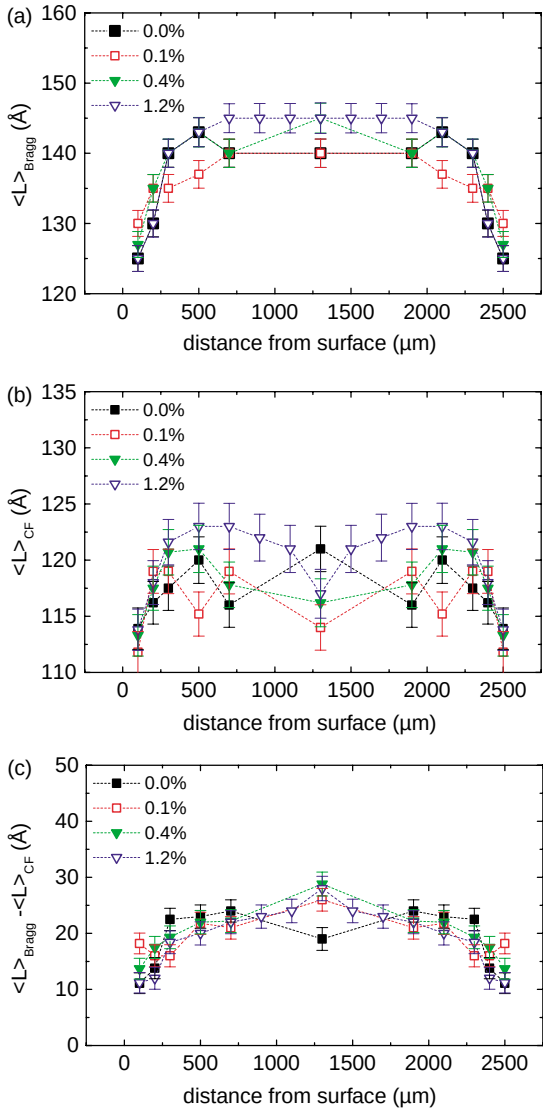

Fig. 9. Distributions of long spacing $\langle L\rangle$ through the depth direction of injection-moulded iPP plates. $\langle L\rangle$ was obtained from the meridional direction. (a) Distributions of $\langle L_{Bragg}\rangle$ obtained from Lorentz-corrected intensity profiles, (b) distributions of $\langle L_{CF}\rangle$ obtained from one dimensional correlation function, and (c) distributions of $(\langle L_{Bragg}\rangle - \langle L_{CF}\rangle)$.

This internal distribution of $\langle L\rangle$ is found not to change in the presence of SB. This can be evidenced by the observation that the distribution of $(\langle L_{Bragg}\rangle$-$\langle L_{CF}\rangle)$ is almost independent of the concentration of SB, as seen in Fig. 9(c).

The assignments of lamellar thickness cannot be done from the analysis of the correlation function because $\langle L_c\rangle$ cannot be distinguished from $\langle L_a\rangle$. The degree of linear crystallinity x_l is related to the degree of volume crystallinity x_v by [35–37]

$$x_v = \varphi x_l \tag{8}$$

where ϕ is the volume fraction of the lamellar stacks in a sample. The value of the fraction ϕ is equal to unity if the whole volume of a sample is perfectly filled with lamellar stacks. Since, the volume outside the lamellar stacks is always filled with amorphous material, x_v is always smaller than x_l. x_v was calculated using wide-angle X-ray data in the conventional

way [38]. All the values of x_v obtained are greater than 0.54. In the surface region, the maximum value of x_v can be as high as 0.65. If the values of $\langle L_1 \rangle$ obtained were assigned as those of $\langle L_c \rangle$, the corresponding values of x_l would have been 0.25–0.3. Apparently, the assumption of $x_l \langle$ 0.5 is physically not valid because $x_l \langle x_v$ suggests that more than 100% space is filled with lamellar stacks. On the basis of the above analysis, $\langle L_2 \rangle$ and $\langle L_1 \rangle$ should be denoted as $\langle L_c \rangle$ and $\langle L_a \rangle$, respectively. x_l is always greater than 0.5 in the present work. The significant increase in $\langle L \rangle$ of iPP-1.2 is thus mainly ascribed to the increase in $\langle L_c \rangle$ (Fig. 10).

Fig. 11 shows the distribution of x_l calculated by Eq. (7) through the depth. The values of x_l calculated by Eq. (6) are somewhat greater than those in Fig. 11. An almost flat distribution of x_l is observed. In general, the values of x_l of iPP-1.2 are greater than those of iPP-0.0 in the broad range of the core. It is worth noting that the SB-enhanced lamellar orientation in the core region is not necessarily accompanied by the increase in x_l.

The background intensity I_b and the equatorial scattering obtained from the core center (1300 μm) of iPP-0.0, $I_{e0,1300}$, were subtracted from the equatorial scattering I_e obtained at the positions of shear region. Since, the total scattering from the core centre without SB contains the contributions from the amorphous chains and unoriented crystalline, the subtraction means that the contribution only from the shish scattering is considered. The concentration of shish is not high and the interference effect between shishes would be limited. Under these conditions, the thickness of shish lamellae was estimated,

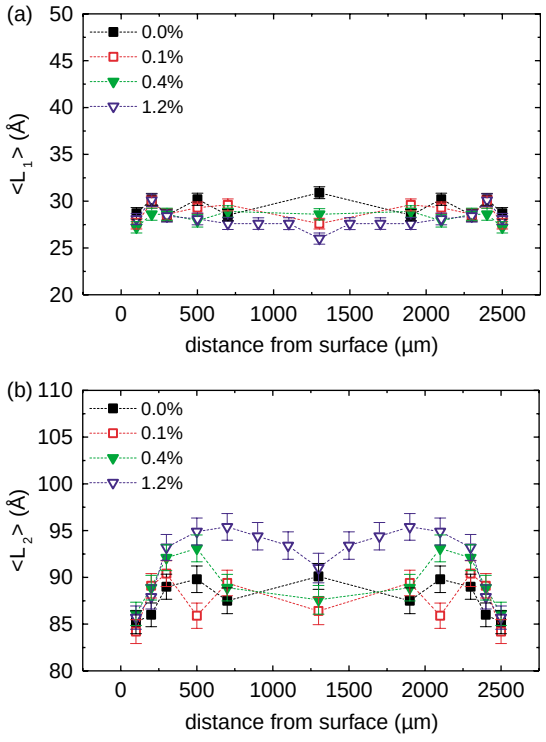

Fig. 10. Distributions of thickness of amorphous lamellae (a) and thickness of crystalline lamellae (b) through the depth direction of injection-moulded iPP plates. $\langle L_1 \rangle$ and $\langle L_2 \rangle$ were obtained from the meridional direction.

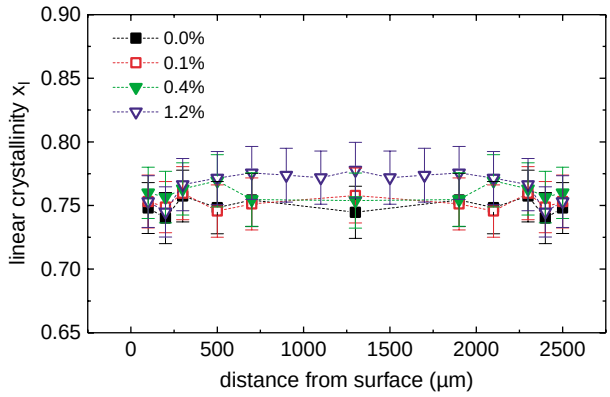

Fig. 11. Distributions of degree of linear crystallinity through the depth direction of injection-moulded iPP plates.

as a first approximation, by a Guinier plot. The equatorial scattering $(I_e - I_b - I_{e0,1300})$ at small q in the Guinier plot is related to the radius of individual rod-like scatterers by the following equation [39]:

$$I_e(q) - I_b - I_{e0,1300}(q) = K \exp\left(-\frac{q^2 R^2}{4}\right) \quad (9)$$

where R is the radius of scattering cylinders in a direction perpendicular to the flow direction, and K is a constant. This Guinier plot was originally derived on the assumption that the concentration of particles is low. The theory can be applied to a more concentrated system provided that all the particles are not similar in shape [39].

Fig. 12 shows the distribution of the shish diameter D_s through the depth. A number of findings can be seen. First, D_s is greater than $\langle L_c \rangle$, regardless of SB. Second, as the concentration of SB increases, the distribution of D_s is changed from a decline to a flat toward the core center. In other words, D_s is strongly dependent on the level of shear flow imposed on iPP-0.0 and iPP-0.1 but independent of the shear flow on iPP-0.4 and iPP-1.2. Third, the variation of D_s with SB is complicate at 100 and 200 μm; for example, the shish diameters obtained from iPP-0.0 are greater than those obtained from other samples.

The emergence of the shish–kebab structure in the depths at which this oriented structure is not observed in the absence of

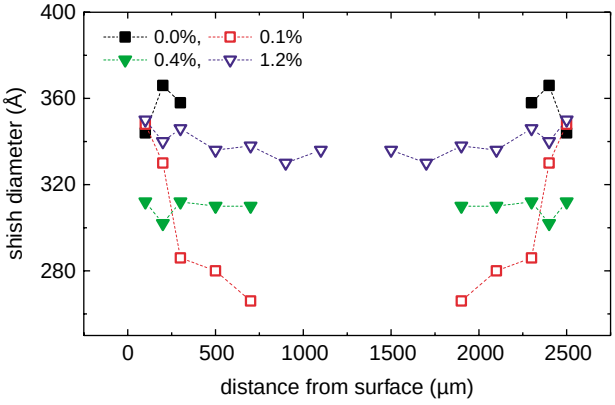

Fig. 12. Distributions of shish diameter through the depth direction of injection-moulded iPP plates.

SB indicates that the shear flow should exist over a much broader range than normally thought. Since, the flow is absolutely essential for the formation of the shish, the forgoing results obtained should be related the effects of SB on the formation of the shish under lower levels of the shear flow. In the absence of SB, since the shear flow attenuates rapidly with the depth, the level of the shear flow is lower than a critical value that can effectively induce the coil-to-stretch transition of chains in the melt. This local orientation is involved in a hysteresis of chains [7]. The relaxation time of chains plays a role in the coil-to-stretch transition. Some of chains that can potentially undergo the conformational transition would be hindered by unstretched chains or due to long relaxation times. The shish crystallization in the absence of SB does not occur in the inner core range 500–1100 μm and the isotropic features of iPP-0.0 image patterns are observed in these depths.

The presence of SB molecules does not bring about any change in the shear flow field. However, the addition of SB can provide a lower surface free energy barrier for the nucleation. The time required to undergo the coil-to-stretch transition would be shortened. In terms of the mechanism proposed by Dukovski and Muthukumar [7], it is suggested that polymer chains would drift more easily in the presence of SB. At low levels of the shear flow, polymers can be induced by the shear in the presence of SB and drift together to form an overlap region consisting of stretched segments. Once these overlap regions form, they can spread rapidly along the entire chains to their maximum possible length, leading to the formation of a complete shish [7]. The shishes formed as nuclei subsequently initiate an epitaxial growth of folded chain kebabs or lamellae. The possible process of the shish formation is schematically presented in Fig. 13. The distribution of shish diameter shows that under the same level of shear flow, the number of iPP-0.0 and iPP-0.1 chains drifting to form an overlap region would be smaller than those of iPP-0.4 and iPP-1.2. The surface free energy barrier and the time required to undergo the conformational transition in the melt should attribute to this difference. When the concentration of SB exceeds a certain value, the number of iPP chains drifting to form an overlap region is independent of the level of the shear flow.

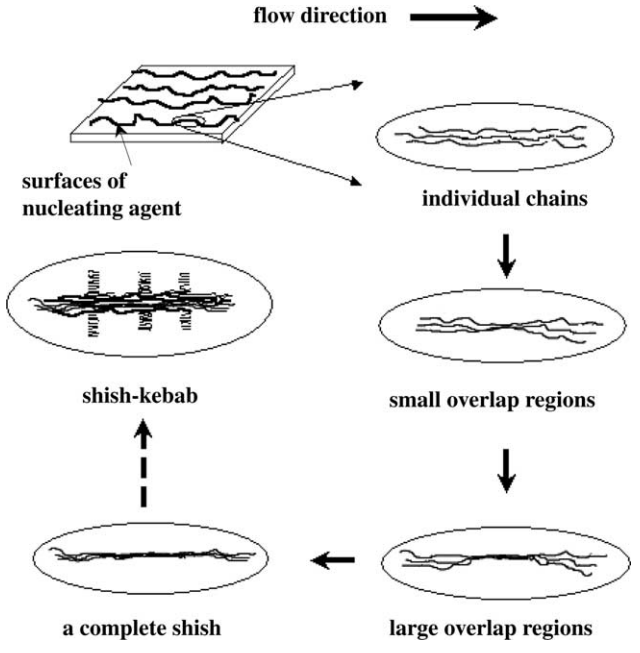

Fig. 13. Illustration of a possible mechanism of shish formation on the surface of nucleating agent molecules in terms of Ref. [7] under weak levels of shear.

In the study of crystallization of sheared iPP in the presence of dibenzylidene sorbitol (DBS), Nogales et al have attributed the anisotropic crystallization of sheared iPP to the formation of oriented assemblies of DBS [40]. Jang et al. have reported that in the presence of SB, the increase in the crystallinity of injection-moulded iPP is accompanied by a significant improvement of the impact strength [41]. Since, a higher degree of crystallinity normally leads to a lower impact strength, Jang et al. have interpreted their findings as a consequence of the formation of interpenetrating physical network due to the existence of SB [41]. The formation of oriented assemblies of SB is not an impossible proposition. The oriented assemblies have locally a higher surface area and would template or direct the formation of shishes under lower levels of the shear flow.

The effects of temperature on the formation of the shish should be taken into account. The important temperature-related parameters to consider in injection moulding include the temperature gradient (or the cooling rate) of the moulding, and the crystallization temperature of the samples, denoted T_c. The temperature in the surface region is lower because the hot melt is much closer to the cold walls of the die, which is acting as a heat sink. The formation of the shish–kebab structure is well understood in this region, which is attributed to a complex combination of the shear flow and rapid cooling [1–3]. In the present work, since the shish–kebab structure appears not only in the surface region but also emerges in a broader range where the cooling rate is lower, it is important to consider the effects of SB on the T_c of iPP. The T_c of iPP increases with increasing concentration of SB [38,41]. For example, T_c of iPP-1.2 is about 11 °C higher than that of iPP-0.0 [38]. For iPP with a saturated concentration of SB, T_c is 15 °C higher than that of iPP without SB [41]. The flow-induced segment orientation occurs when the time to reach T_c, (denoted t_c), is shorter than the time required for the molecular relaxation, t_r [18]. This is because the polymer segments do not have enough time to undergo complete molecular relaxation before crystallization. Once the flow-induced crystallization starts, polymer segments are locally constrained in ordering surroundings. Note that if t_c were longer than t_r, polymer chains would relax to crystallize into a spherulitic-like structure [18]. Since, T_c of iPP is increased by the addition of SB, t_c is shortened. Some oriented segments are expected to form in the core region at higher temperatures. These oriented segments can act as the shishes to generate the epitaxial growth of polymer chains over a broader range of the depth, as is observed.

The formation of an insulation barrier due to the low thermal conductivity of iPP leads to slower cooling rates in the core region. The slower cooling rate in the core region allows a more complete relaxation of chains during crystallization, which can

lead to an increase in the thickness of crystalline lamellae. The results herein show that the thickness of the crystalline lamellae occurs only when the concentration of SB is sufficiently high, in this case only for iPP-1.2. Thermodynamically, the effect of temperature on the thickness of a crystalline lamella, as a simplest level, can be given as follows [42]

$$\langle L_c \rangle = \frac{2\sigma_e}{\Delta H_m} \frac{T_m^0}{T_m^0 - T_c} \tag{10}$$

where σ_e is the fold surface (basal interface) enthalpy, ΔH_m is the melting enthalpy per unit volume, T_m^0 is an equilibrium melting temperature, T_c is the crystallization temperature, and $\Delta T = (T_m^0 - T_c)$ is the degree of the supercooling corresponding to T_c. The fold surface enthalpy σ_e is proportional to the concentration of a nucleating agent [43,44]. The fold surface enthalpy would be locally decreased in the presence of nucleating agents and the thickness of crystalline lamellae should accordingly decrease at a given T_c. On the other hand, the higher crystallization temperature T_c or the lower value of supercooling ΔT in the presence of nucleating agents would lead to an increase in the thickness of crystalline lamellae. Overall, in terms of Eq. (10), these contributions play opposed roles. The thickness of crystalline lamellae is determined by the consequence of this intricate balance.

4. Conclusions

The effects of sodium benzoate on the distributions of lamellar structures of injection-moulded iPP plates were investigated using synchrotron small-angle X-ray scattering. The iPP specimens were cut from the centre of each plate, and the experiments were designed in such a way that a 200× 200 μm^2 square beam vertically passed through the section and the illuminated zone at a given distance from the surface of a plate was accurately changed with a vertical shift of the sample holder through the thickness. The lamellar structures obtained include the shish–kebab structure, lamellar orientation, long spacing, thickness of crystalline lamellae, and thickness of amorphous lamellae. The corresponding distributions of these structures are then constructed through the thickness of plates.

The results show that the shish–kebab structure of sheared iPP can be enhanced by the presence of SB under the same level of shear flow field. More importantly, with increasing concentration of SB, the shish–kebab structure is found over a broader range of the depth. The addition of SB provides lower free energy barriers for the coil-to-stretch transition or the shish crystallization. The emergence of the shish–kebab structure in the presence of SB is also ascribed to the shorter time to start the crystallization of iPP. Once the shishes form, they can generate the epitaxial growth of the kebabs or folded chain lamellae by the way of a periodic match. Since, the shish cannot form in the absence of flow, the emergence of the shish–kebab structure in the low levels of shear flow field implies that the SB can act like a molecular probe to trace a true range of shear flow field.

With decreasing shear flow through the thickness of the plate, the size of shish decreases at lower concentrations of SB, whereas the size of shish remains a constant at higher concentrations of SB. As a direct consequence of the formation of the shish–kebab structure, the level of the preferential orientation of crystalline lamellae is significantly increased over the core range, although the orientation in the surface region is not much influenced by SB.

The addition of SB does not alter the distribution of the long spacing through the depth. It is found that the distribution of long spacing is mainly ascribed to the variation of $\langle L_c \rangle$ with the depth. The effect of SB on the lamellar dimensions becomes significant only in the core region of iPP-1.2. $\langle L_c \rangle$ of iPP-1.2 increases whereas its $\langle L_a \rangle$ slightly decreases. The degree of linear crystallinity of iPP-1.2 is accordingly increased. The cooling rate would play a dominant role in enhancing the thickness of crystalline lamellae. A higher level of lamellar orientation does not necessarily correspond to a higher degree of linear crystallinity.

Acknowledgements

This work was performed at the Australian National Beamline Facility (ANBF) with support from the Australian Synchrotron Research Program, which is funded by the Commonwealth of Australia under the Major National Research Facilities Program. Dr James Hester (ANBF) is greatly acknowledged for his assistance in the experiments. P. W. Zhu wishes to thank Dr Fujiyama for very fruitful discussion.

References

[1] Meijer HEH, editor. Processing of polymers, vol. 18. Germany: Weinheim; 1997.
[2] Janeschitz-Kriegl H. Colloid Polym Sci 2003;281:1157.
[3] Keller A, Kolnaar HWH. In: Meijer HEH, editor. Flow induced orientation and structure formation. Processing of polymers, vol. 18. Germany: VCH, Weinheim; 1997.
[4] Lee O, Kamal MR. Polym Eng Sci 1999;39:236.
[5] Kumaraswamy G, Issaian GA, Kornfield JA. Macromolecules 1999;32: 7537.
[6] Rueda DR, Ania F, Balta-Calleja FJ. Polymer 1997;38:2027.
[7] Dukovski I, Muthukumar M. J Chem Phys 2003;118:6648.
[8] Seki M, Thurman DW, Oberhauser JP, Kornfield JA. Macromolecules 2002;35:2583.
[9] Nogales A, Hsiao BS, Somani R, Srinivas S, Tsou AH, Balta-Calleja F, et al. J Polym 2001;42:5247.
[10] Hu W, Frenkel D, Mathot VBF. Macromolecules 2002;35:7172.
[11] Gu F, Bu H, Zhang Z. Macromolecules 2000;33:5490.
[12] Hill MJ, Barham PJ, Keller A. Colloid Polym Sci 1980;258:1023.
[13] Hill MJ, Barham PJ, Keller A. Colloid Polym Sci 1983;261:721.
[14] Zipper P, Janosi A, Geymayer W, Ingolic E, Fleischmann E. Polym Eng Sci 1996;36:467.
[15] Fujiyama M, Kimura S. J Appl Polym Sci 1978;22:1225.
[16] Katti SS, Schultz JM. Polym Eng Sci 1982;22:1001.
[17] Eder G, Janeschitz-Kriegl H. Colloid Polym Sci 1988;266:1087.
[18] Viana JC, Cunha AM, Billon N. Polymer 2002;43:4185.
[19] Gao X, Isayev AI, Guo L. Polym Eng Sci 1999;39:2096.
[20] Eder G, Janeschitz-Kriegl H, Liedauer S. Prog Polym Sci 1990;15:629.
[21] Ania F, Bayer RK, Tschmel A, Michler HG, Naumann I, Balta-Calleja FJ. J Mater Sci 1996;31:4199.
[22] Andersen PG, Carr SH. J Mater Sci 1975;10:870.
[23] Lovinger AJ. J Polym Sci, Polym Phys Ed 1983;21:97.

[24] Fujiyama M, Wakino T, Kawasaki Y. J Appl Polym Sci 1988;35:29.
[25] Lotz B, Wittmannn JC. J Polym Sci, Polym Phys Ed 1986;24:1541.
[26] Zhu PW, Edward G. Macromolecules 2004;37:2658.
[27] Mathieu C, Thierry A, Wittmann JC, Lotz B. Polymer 2000;41:7241.
[28] Schultz JM, Hsiao BS, Samon JM. Polymer 2000;41:8887.
[29] White HM, Bassett DC. Polymer 1997;38:5515.
[30] Strobl GR. The physics of polymers. New York: Springer; 1997.
[31] Ruland W. J Appl Cryst 1971;4:70.
[32] Vonk CG, Kortleve G, Kolloid Z-Z. Polymer 1967;220:19.
[33] Koberstein J, Stein JR. J Polym Sci, Polym Phys Ed 1983;21:2181.
[34] Ruland W. Acta Cryst 1961;4:1180.
[35] Santa-Cruz C, Stribeck N, Zachmann HG, Balta-Calleja FJ. Macromolecules 1991;24:5980.
[36] Verma RK, Marand H, Hsiao BS. Macromolecules 1996;29:7767.
[37] Medellin-Rodriguez FJ, Phillips PJ, Lin JS, Campus R. J Polym Sci, Polym Phys 1997;35:1757.
[38] Zhu PW, Tung J, Phillips AW, Edward GH. Manuscript in preparation.
[39] Guinier A, Fournet G. Small-angle scattering of X-rays. New York: Wiley; 1955.
[40] Nogales A, Mitchell GR, Vaughan AS. Macromolecules 2003;36:4898.
[41] Jang GS, Cho WJ, Ha CS. J Polym Sci, Polym Phys Ed 2001;39:1001.
[42] Donth EJ. Relaxation and thermodynamics in polymers. Berlin: Akadenie; 1992.
[43] Pieruccini M, Macro GD, Lanza M. J Appl Phys 1996;80:1852.
[44] Aliotta F, Macro GD, Pieruccini M. Physica A 2001;298:266.